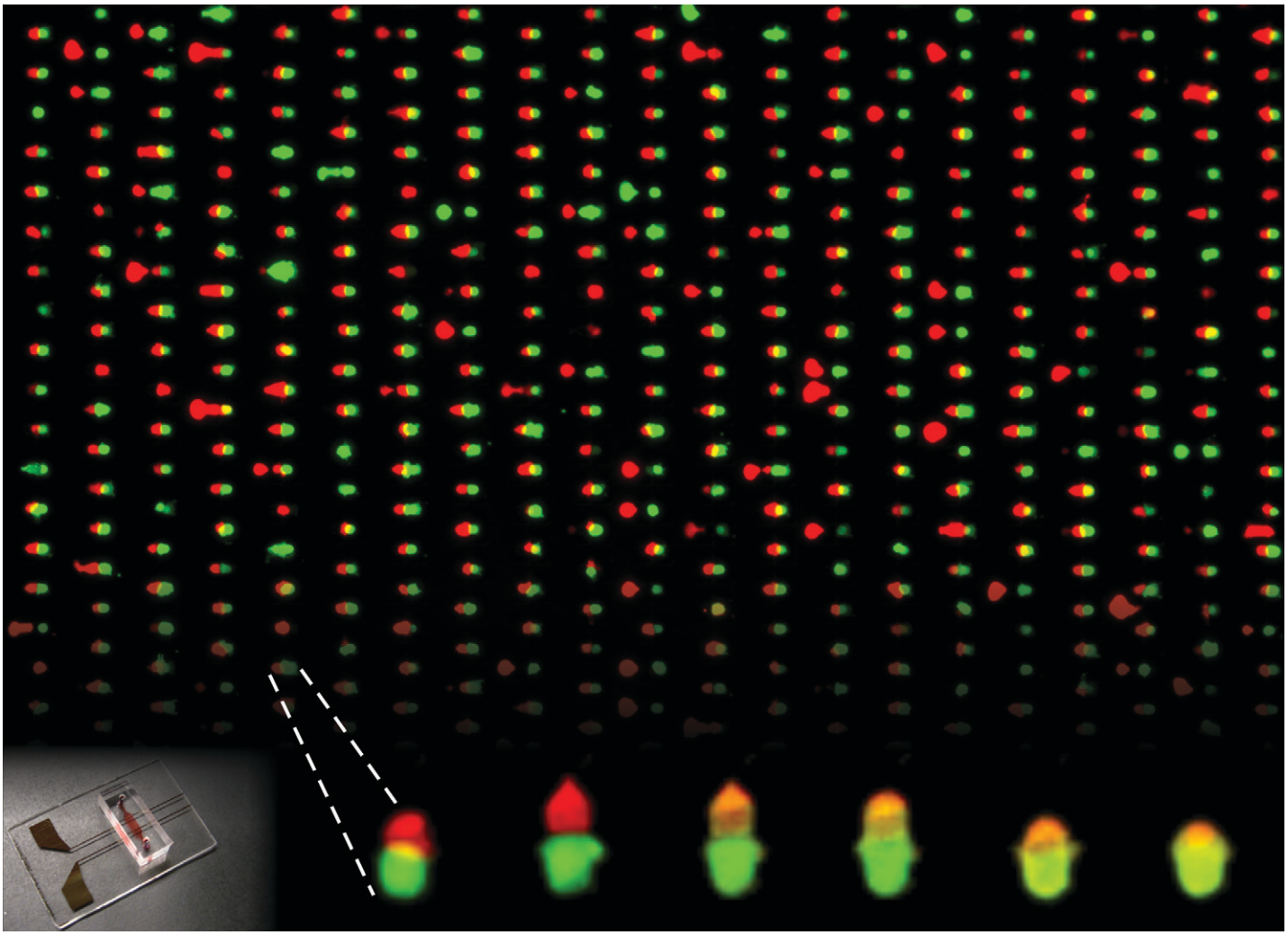

Featuring work from the group of Professor Joel Voldman in the Department of Electrical Engineering and Computer Science, Massachusetts Institute of Technology, Cambridge, MA, USA.

Title: Deformability-based microfluidic cell pairing and fusion

A novel microfluidic platform for sequential trapping and pairing of cells in parallel by passive hydrodynamics and flow-induced deformation. Immobilized cell pairs can be fused using biological, chemical or physical stimuli, achieving a five-fold to fifteen-fold improvement in fusion yields in comparison to commercial systems.

As featured in:

See Joel Voldman *et al.*, *Lab Chip*, 2014, **14**, 2783.

ROYAL SOCIETY OF CHEMISTRY

www.rsc.org/loc

Registered charity number: 207890

Lab on a Chip

PAPER

View Article Online
View Journal | View Issue

Deformability-based microfluidic cell pairing and fusion†

Cite this: *Lab Chip*, 2014, **14**, 2783

Burak Dura, Yaoping Liu and Joel Voldman*

Received 9th March 2014,
Accepted 20th May 2014

DOI: 10.1039/c4lc00303a

www.rsc.org/loc

We present a microfluidic cell pairing device capable of sequential trapping and pairing of hundreds of cells using passive hydrodynamics and flow-induced deformation. We describe the design and operation principles of our device and show its applicability for cell fusion. Using our device, we achieved both homotypic and heterotypic cell pairing, demonstrating efficiencies up to 80%. The platform is compatible with fusion protocols based on biological, chemical and physical stimuli with fusion yields up to 95%. Our device further permits its disconnection from the fluidic hardware enabling its transportation for imaging and culture while maintaining cell registration on chip. Our design principles and cell trapping technique can readily be applied for different cell types and can be extended to trap and fuse multiple (>2) cell partners as demonstrated by our preliminary experiments.

Introduction

Cell fusion is a natural process that occurs during embryogenesis,[1,2] development[3–5] and immune responses,[6–8] and has further been implicated in the progression of cancer[9–11] and in tissue regeneration by stem cells.[12] Fusion of cells can also be induced artificially by application of a biological, chemical or physical fusogen and has become a routine laboratory technique for monoclonal antibody production,[13] cancer immunotherapy[14] and nuclear reprogramming of somatic cells.[15]

Overall fusion efficiency is largely predicated on the fusogenicity of the partner cells. Choice of optimal fusion method will therefore depend on cell intrinsic properties and feasibility for the application. Regardless of the fusion method, one major determinant of fusion efficiency is the formation of stable cell contacts between partner cells. Standard fusion methods rely on random cell pairings and have unstable cell–cell contacts, which often yields low efficiencies and unwanted fusion products requiring selection and isolation of desired hybrids.[13,16] To address this issue, we and others have developed microfluidic approaches for controlled pairing of partner cells prior to fusion using chemical,[17,18] hydrodynamic,[19,20] and dielectrophoresis-based approaches,[21–23] and have demonstrated increased fusion efficiencies up to 90% for various types of cells. Despite their capabilities, present platforms have several limitations that motivate the development of improved fusion methods. First, many methods are compatible with only a subset of fusion methods due to their intrinsic operation; for example, platforms based on electrical manipulation[21–23] can only operate with solutions of certain conductivity and osmolarity which render them incompatible with chemical and viral fusogens that require media exchange. Similarly, flow-through approaches such as based on chemical conjugation[18] do not allow solution exchange and have only been demonstrated for electrofusion. Compatibility with a variety of fusion protocols would better accommodate inherent differences in the fusogenicity of partner cells as one method might be superior to another, and would also enable co-application of a subset of fusogens.[24] A second important limitation is that existing methods do not permit disconnecting the platform from the external hardware without losing registration of fused cells, which in turn prevents transportation of the sample to different experimental settings for long-term studies. Third, existing platforms do not possess the potential for extension to multiple (>2) cell capture, which would enable formation of multinucleated cells for studying developmental biology (muscle cell fusion), immunology (giant multinucleated leukocytes), and gene dosage in nuclear reprogramming.

Here we describe a microfluidic deformability-based cell pairing device densely packed with silicone hydrodynamic traps in a flow-through channel. The novel trap design allows sequential trapping and pairing of hundreds of cells at once by passive hydrodynamics and flow-induced deformability. Using our device, we demonstrate creation of both homotypic and heterotypic cell pairs, achieving pairing efficiencies up to

Department of Electrical Engineering and Computer Science, Massachusetts Institute of Technology, 77 Massachusetts Avenue, Room 36-824, Cambridge, MA 02139, USA. E-mail: voldman@mit.edu; Fax: +1 617 258 5846; Tel: +1 617 253 1583

† Electronic supplementary information (ESI) available: Fig. S1, Movie S1, Movie S2. See DOI: 10.1039/c4lc00303a

80%. After cell pairing, the cell pairs are secured in their traps, allowing the device to be disconnected from the fluidic hardware without losing the registration of cell pairs on the chip. We further demonstrated the utility of our device for cell fusion using biological, chemical and physical fusogens, yielding fusion efficiencies up to 95%. Finally, we show initial results that suggest the extendibility of this pairing and fusion technique to multiple cell partners (>2) for generation of multinucleated hybrids.

Results and discussion

Microfluidic device design

The device contains hundreds of weir-based silicone (polydimethyl siloxane; PDMS) hydrodynamic traps arrayed within a flow-through channel (Fig. 1a, b) and attached to a glass capping substrate. The cell trapping structure consists of a single-cell trap connected to a double-cell trap through a constriction (Fig. 1c, d), and its dimensions were chosen based on the mean diameter of the cell populations to increase the fractional flow rate through the trapping structure *versus* around the structure. Support pillars placed on each side of the traps along with openings in the middle of each sidewall provide fluid flow through the cups to direct cells into traps, and were chosen smaller than the cell radius to avoid cells from squeezing out of the traps, especially with increased flow rates during the cell loading procedure. The single-cell trap was tailored smaller than cell diameter to ensure capture of only one cell. We sized the double-cell trap (width, depth, constriction) to accommodate the chosen cell pairs of interest with proper alignment within the trap. The support pillar at the back of the double-cell trap ensures cell entrapment once the cells are in the cups.

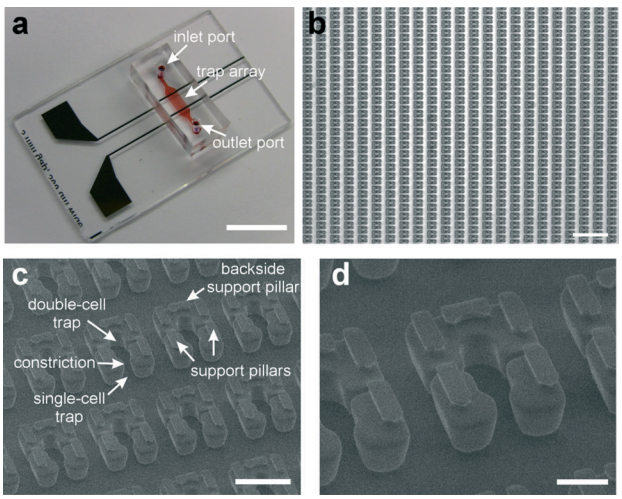

Fig. 1 Microfluidic device for deformability based cell pairing. (a) Image of the microfluidic device bonded to a glass slide patterned with electrodes. Channel and trap array are shown in red. (b) Phase image of the device showing the arrangement of the traps within the array. (c, d) Scanning electron micrograph images of the device detailing the trap structure. Scale bars (a) 10 mm, (b) 500 μm, (c) 50 μm, (d) 20 μm.

The optimal device design requires proper choice of trap spacings within the array to maximize capture efficiency defined as the ratio of the number of cells captured to total cells entering the device. The row and column spacing between the trapping structures were thus set empirically to balance between maximum capture efficiency and minimal clogging. With this choice of design parameters (row spacing 2–2.5× cell diameter; column spacing 1.2–1.5× cell diameter), we could achieve highly synchronous (<60 s) and sample-efficient ($\sim 10^4$ cells) loading of the single-cell traps with >95% of the single-cell traps occupied (~750–900 traps in $\sim 2 \times 3$ mm^2).

Deformability-based cell capture and pairing

Once cells are captured in the single-cell traps, cell pairing occurs by transferring those cells into the double-cell traps. The overall capture and pairing approach used a four-step loading procedure. The first cell population was initially captured in the single-cell trap by passive hydrodynamics (Fig. 2a-1). With optimal row spacing (20–30 μm; ~1–1.5 cell diameters) and column spacing (~20 μm) of the traps, we could capture 50–80% of the cells that entered the array without any clogging issues. Once the array was saturated (typically <60 s), additional cells were washed out of the device and flow rate was briefly increased to squeeze the cells from the single-cell trap into the larger double-cell traps through the constriction by flow-induced deformation (Fig. 2a-2). This step was fast (~1–2 s) and highly parallel, occurring across the entire array within ~s. Loss of cells during this step was minimal (<5%) and prevented by proper choice of trap dimensions (height of support pillar layer) and backside support pillars that help maintain the cells within the traps even against increased flow rates. Next, the second cell population was introduced into the device to capture them in the single-cell traps (Fig. 2a-3) and then squeeze them into the larger traps in a similar fashion to achieve cell pairing (Fig. 2a-4). Sizing the double-cell trap geometry just large enough to accommodate the two cells ensured that the cells were pre-aligned and remained in contact once paired. Using NIH3T3 fibroblasts, we achieved cell pairing efficiencies between 50–80% (mean 63 ± 8%; n = 16, Fig. 2b).

Once the pairing is completed, the cells are immobilized and secured in their traps due to the small constriction, allowing the device to be disconnected from the fluidic hardware without losing the registration of cell pairs on the chip (Fig. 2b, c; cell pairs preserved 100–87%). This lock-in feature[25] enables the transportation of the device for further studies (*i.e.*, imaging) and/or transfer to a standard incubator for long-term culture (Fig. 2d), eliminating the need for on-stage incubator setups. We observed that although cell pairs remain within their traps after disconnection, they could migrate out of their traps upon culturing on chip. We envision that cell pairs could further be confined to grow within the traps using cell-adhesive micro-patterned substrates, which could be useful for controlled positioning of cell pairs for co-culturing and cell–cell interaction studies.[26–28]

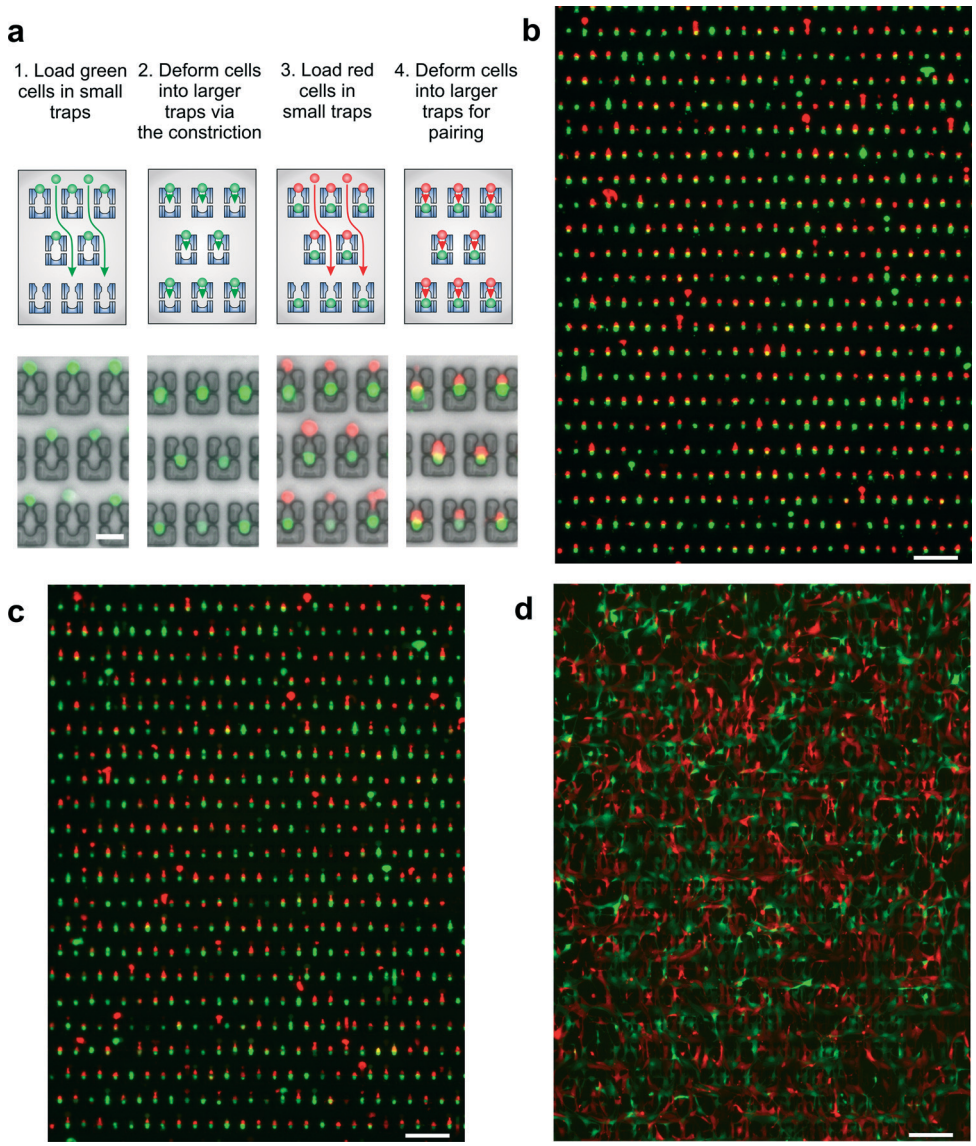

Fig. 2 Cell loading and pairing protocol. (a) 1. First cell population is passively captured in the single-cell traps. 2. Cells are transferred into the larger two-cell traps by flow-induced deformation. 3–4. Using the same protocol, second cell population was trapped immediately in front of the first cell type. (b) Representative fluorescence overlay cell pairing image of the eGFP- and DsRed-expressing NIH3T3 fibroblasts. (c) Lock-in feature. Fluorescence overlay image of NIH3T3 fibroblasts in (b) after disconnection from the external fluidic hardware. (d) Fluorescence overlay image of the cells after two-day on-chip culture. Scale bars (a) 50 μm, (b–d) 200 μm.

In addition to homotypic pairing where cells are of similar sizes, we developed methods for heterotypic pairing where cell sizes can differ substantially. Design principles can be adapted to cells with different sizes by modifying trapping structure geometries; however the choice of parameters can be challenging for pairing cells that are substantially mismatched in size. To facilitate cell pairing for such cases, we developed a modified cell loading procedure by loading the smaller cell population in hypoosmolar buffer, which causes the cells to swell and approximate the size of the larger cell population. By adjusting the osmolarity of the loading solution, cell sizes can be set to suit the trap geometries. Once the cells are passively trapped in the single-cell traps, transfer into the double-cell traps can either be accomplished by flow-induced deformation or by changing the solution back to an isoosmolar one to shrink the cells into the traps. We demonstrated the utility of the modified loading procedure by pairing NIH3T3 fibroblasts (~18 μm) and BA/F3 mouse leukocytes (~10 μm) using the devices tailored for NIH3T3 cells. Initial attempts using the original cell pairing approach resulted in low BA/F3 cell capture efficiency (<10%) due to smaller size and multi-cell pairing as more than one BA/F3 cell can squeeze through the traps even at very low flow velocities (Fig. S1a†). Our modified approach however resolved these issues (Fig. 3a). We first loaded the NIH3T3 fibroblasts as in previously. We then loaded the BA/F3 cells in hypoosmolar buffer, which induced a substantial increase in cell diameter (1.3–1.6×; Fig. 3a, S1b†) and allowed efficient

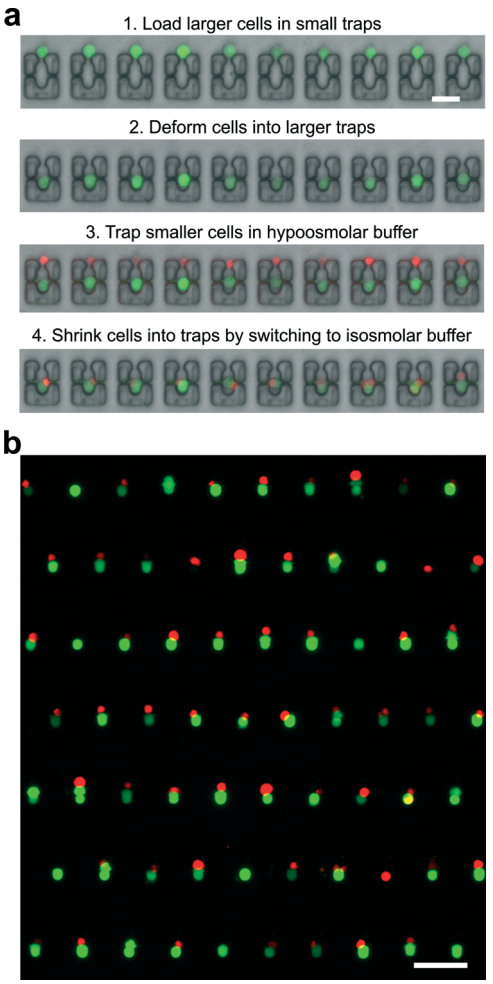

Fig. 3 Osmolarity change-based cell loading protocol. (a) 1. First cell population is passively captured in the single-cell traps. 2. Cells are transferred into the larger two-cell traps by flow-induced deformation. 3. Smaller cells are loaded in hypoosmolar buffer and captured in single-cell traps. 4. Cells are transferred into larger traps by switching to isoosmolar buffer and returning to their original sizes. (b) Representative fluorescence overlay cell pairing image of the eGFP-expressing NIH3T3 fibroblasts and Turbo RFP-expressing BA/F3 mouse leukocytes. Scale bars (a) 50 μm, (b) 100 μm.

capture (>50%). We then switched to isoosmolar media to shrink the cells into the traps to achieve one-to-one cell pairing (Fig. 3a, b). In the case of any remaining cells that did not enter the traps by shrinkage alone, flow rate was increased briefly (~s) to facilitate the transfer of cells into the traps.

Although our loading protocols included brief fluid-induced deformation and/or exposure to hypoosmolar buffer treatment (no longer than 6 min, much less than the exposure times during electrofusion procedures), cells remained highly viable, did not show any discernible morphological changes and proliferated in culture, indicating no significant influence of the procedures on cells. Overall, these results show that our trapping approach combined with an osmolarity change-based cell loading procedure can be used to capture and pair cells of both similar and divergent sizes.

Fusion in microfluidic device

We next demonstrated the applicability of our device for cell fusion. We first evaluated the performance of our device for electrofusion. Devices were plasma-bonded to glass slides containing patterned metal electrodes to apply electric fields (Fig. 1a). After cell pairing was achieved, hypoosmolar buffer was introduced in the device to induce cell swelling (Fig. 3a). After 5 min, an electric-field pulse sequence was applied and cells were kept in hypoosmolar buffer for additional 10 min. Following the incubation time in hypoosmolar buffer, solution was exchanged with cell media and cells were incubated on chip for another 15 min. The overall fusion process was imaged and recorded for characterization of fusion efficiencies (Movie S1†).

We determined the fusion efficiencies by examining the fluorescence exchange over the correctly paired cell partners (eGFP 3T3 paired with DsRed 3T3). With optimized electric field parameters, we achieved electrofusion efficiencies between 78–95% (mean 86 ± 12%, n = 3), yielding overall efficiencies of 56 ± 8% properly paired and fused cells over the entire device (Fig. 4e, f). There are two major advantages of our device for electrofusion. First, cells remain in contact and pre-aligned with the electric field, eliminating the need for alternating current field application for cell alignment. Secondly, as cells are paired in a predetermined volume within the traps, tighter cell contacts are forced mechanically upon cell swelling during infusion with the hypofusion buffer that precedes the electric pulse application. We hypothesize that the mechanically facilitated cell–cell contacts help improve the fusion yields both due to tighter contacts and increased contact surface.[29] The lock-in feature further enables transport of the device into standard incubators for on-chip culture of the fused cells over multiple days (Fig. 4f). Alternatively, cells can also be purged out of the device for off-chip culture by flushing the cells in the opposite direction of cell loading, and squeezing them out of their traps through the constriction. The cells can then be collected in standard multiwell plates for culture and further analysis (Fig. 4g).

In addition to electrofusion, there are three other fusion methods that are commonly employed, namely biological (viral fusion), chemical (PEG-induced) and laser-induced fusion. The main challenge with virus- and PEG-based fusion methods is to maintain cell–cell contacts while successively infusing cells to a variety of solutions specified in the protocol. Another advantage of our device is the ability to rapidly exchange the soluble microenvironment around the cells without impairing the pairing. This feature thus makes our device compatible with both viral and PEG-based fusion methods (Fig. 4b, c). As our device is transparent and can be transported to different experimental settings, our device can also be adapted for laser-induced fusion protocols as well.

Due to nature of the sequential cell trapping, our device and cell loading protocol have potential extendibility for >2 cell partners. We therefore tested the applicability of our

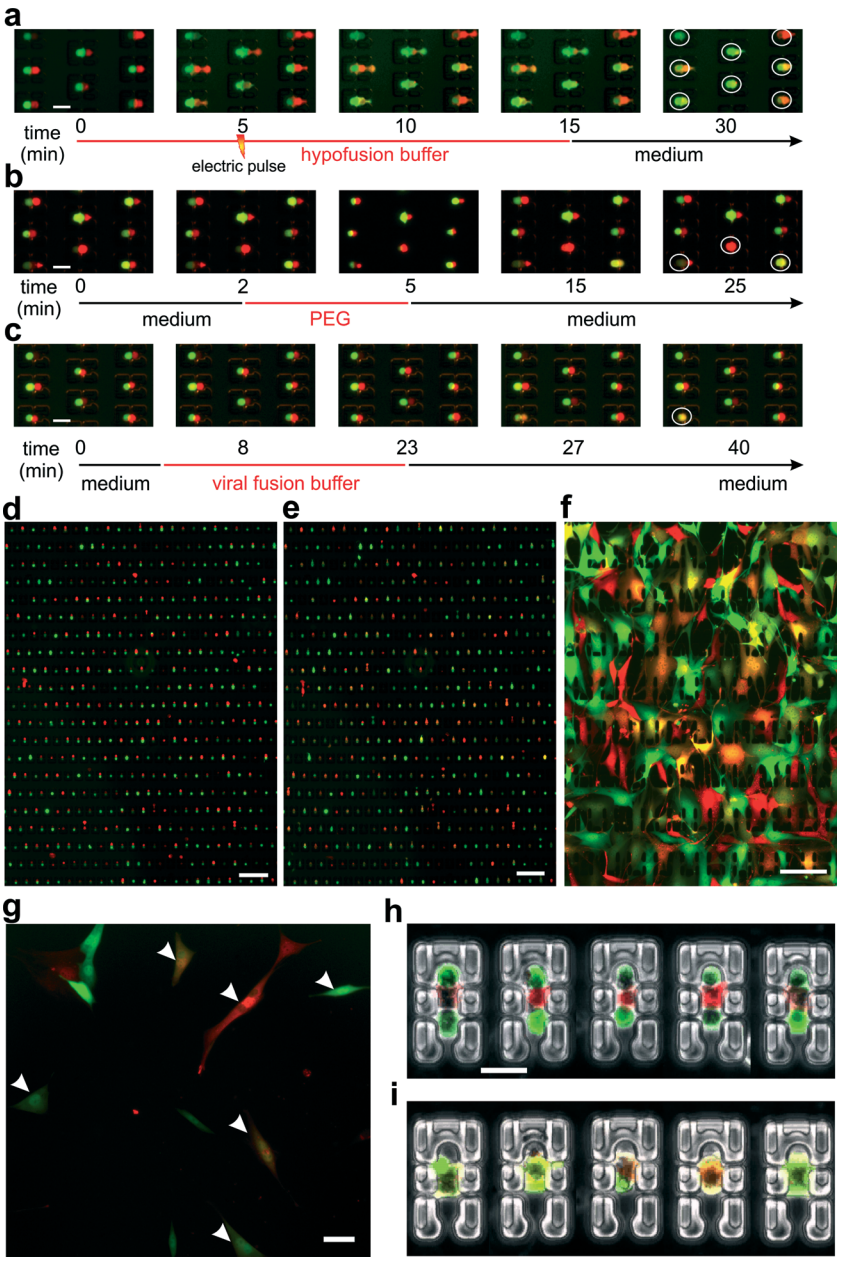

Fig. 4 Fusion in the microfluidic device. (a) Time-course of electrofusion of eGFP- and DsRed-expressing NIH3T3 mouse fibroblasts. During cell swelling with hypofusion buffer, cells are restricted to a predefined area; hence form tighter cell contacts. Exchange of fluorescence is observable immediately after the electric pulse application. Formation of hybrid cells is evident toward the end of experiment by mixed contents of both cells (shown with white circles). (b) Time course of PEG-based fusion of eGFP- and DsRed-expressing NIH3T3 mouse fibroblasts. Fused cells shown with white circles. (c) Time course of viral fusion of eGFP- and DsRed-expressing NIH3T3 mouse fibroblasts. Fused cells shown with white circles. (d, e) Fluorescence overlay image of the entire field of view immediately (b) after pairing, (c) after fusion. (f) Fluorescent overlay images of fused cells after four-day on chip culture. (g) Fluorescent overlay images of fused cells after one-day off chip culture in multiwall plate. Arrows point to fused hybrids determined by the presence of double fluorescence. (h–i) Extension of cell pairing and electrofusion protocol to cell triplets. Five representative NIH3T3 fibroblast triplets that were correctly trapped (h) and fused (i) were chosen and stitched together in a single image. Scale bars (a–c) 50 μm, (d, e) 200 μm, (f) 100 μm, (g–i) 50 μm.

device to trap and fuse multiple cell partners. Our results show that successive trapping and fusion of three cells were possible (Fig. 4h, i; Movie S2†). Although the tripling efficiencies were low (~10%), we anticipate higher tripling efficiencies with further optimization and proper choice of trap geometry and dimensions. These results present the first controlled >2 cell pairing and fusion, and demonstrate the extendibility of our approach. The results also suggest that our sequential cell loading protocol could further enable potential trapping and fusion of >3 cell partners.

Discussion

We have introduced a novel cell pairing approach based on passive hydrodynamics without the need for manipulation methods such as chemical conjugation or alternating electric fields. The trap geometry and design principles can readily be modified and adapted for different cell types and varying number of cell partners. The osmolarity change-based cell loading further adds to the flexibility with respect to the choice of design parameters for divergent cell sizes especially relevant for heterotypic cell pairing. Hence, the presented technique should be generally applicable to a wide range of cell types and sizes. As cells can show variation in their responses to deformation[30] and hypoosmolar buffer treatment,[31] the fluid-flow rates (for deformation) and exposure times to hypoosmolar buffer should be selected optimally by preliminary tests for cell types of interest to induce minimal stress during loading procedures.

Compared to previous designs,[18,21–23] our devices allow for immobilization of cell pairs within their traps, thus enabling rapid media exchange and making it compatible with biological, chemical and electrical fusion protocols. In particular, electrofusion efficiencies in our devices were between 78–95% with overall yields of 56 ± 8% properly paired and fused cells, which represents a five-fold to fifteen-fold improvement over the yields we and others previously reported using commercial systems (4–11%,[19] 5–20%[32]). Further improvements might be possible with novel fusion techniques such as co-application of a subset of fusogens.

The immobilization of the cells within their traps also allow on-chip cell culture with sample transfer functionality. These features would enable longitudinal studies over the cell pairs or fused cells (such as fusion-mediated reprogramming events[33]) across different experimental settings while maintaining their histories. Alternatively, fused cells can also be harvested from the device for standard cell culture and conventional assays (*e.g.* hybridoma screening,[13] dendritic cell/tumor cell fusion vaccines[14]). Apart from fusion, the devices also permit dynamic monitoring from the exact moment of membrane contact. Therefore, our devices can also be used to gain insight into dynamics of cell–cell interactions particularly prevalent among immune cells. Trapped pairs can be exposed to varying environmental inputs, and their responses can be monitored over time. Such dynamic imaging studies at high throughputs in controlled microenvironments would likely yield new insights that are otherwise averaged out in conventional assays.

Conclusions

We presented a microfluidic device capable of sequential trapping and pairing of cells with similar and divergent sizes. We further showed the utility of our device for fusion using biological, chemical and physical stimuli. In addition to high pairing/fusion efficiencies and compatibility with a variety of fusion methods, our pairing method also enables the transportation of the device for imaging and long-term culturing while maintaining cell registration and is extendible to multiple cell partners as demonstrated by our preliminary results. The trap geometry and design principles can readily be modified and adapted for different cell types and varying number of cell partners. With its unique features, we envision the use of our devices not only for hybrid generation but also for characterization of fusion events relevant to development biology, immunology and nuclear reprogramming as well as for co-culturing and cell–cell interaction studies in immunology and tissue engineering.

Experimental

Microfluidic device fabrication

Microfluidic devices were fabricated by soft lithography. Masters for the microfluidic devices were fabricated using a two-layer SU8 process. SU-8 2005 photoresist (MicroChem, Newton, MA) was spun at 2000–3000 rpm for 30 s to yield the first layer with feature heights of 4–5 μm. The wafers were UV-exposed to through a chrome mask with support pillar patterns (Advance Reproductions, North Andover, MA). After developing and baking following manufacturer's protocol, the second layer of photoresist (SU-8 2015) was spun at 2000–2500 rpm for 30 s to yield feature heights of 18–20 μm. The wafers were then UV-exposed through a second chrome mask with cell trap patterns. Following developing and baking, SU-8 molds were hard-baked at 150 °C for 30 min, and were treated with Trichloromethylsilane (Sigma-Aldrich, St. Louis, MO) for 2 h in a saturated vacuum chamber to prevent adhesion of polydimethyl siloxane (PDMS; Sylgard 184, Dow Corning, Midland, MI) during the molding process.

Devices were cast by pouring PDMS over the master wafers followed by degassing and curing at 80 °C overnight. PDMS was then peeled off, and individual devices were cut to proper sizes. Holes for fluidic connections were punctured using hole punchers.

Glass slides with patterned electrodes were fabricated from mask blanks pre-coated with chrome and photoresist (Telic, Valencie, CA). Electrode patterns are transferred to mask blanks through a transparency mask (Page Works, Cambridge, MA) and developed in NaOH. The remaining photoresist was stripped off using acetone. The PDMS devices were plasma-bonded to glass slides with proper alignment of trap array and electrodes. Wires were bonded to the chrome electrode pads using conductive epoxy (MG Chemicals, Surrey, BC, Canada) for connection to electrical signal generator.

Microfluidic setup and cell pairing procedure

Microfluidic devices were initially filled with 70–80% ethanol to facilitate bubble-free filling. The surfaces were blocked using 7.5% BSA (37 °C, >30 min). After the assembly of fluidic connections, devices were rinsed with cell media before introducing the cells. Tygon Microbore tubing (Cole Parmer, Vernon Hills, IL) connected to a 4-way valve (UpChurch Scientific, WA) was plugged into the outlet of the device. The valve

was also connected to two 1 mL glass syringes (Hamilton, Reno, Nevada) on two separate syringe pumps. One syringe pump was used to provide flow at 0.2–2 μL min^{-1} for infusion of solutions and passive trapping of cells. The other pump was operated at high flow rates (100–500 μL min^{-1}) to deform cells into traps by increased fluidic pressure during cell loading. Devices were used in an open reservoir format where cells and reagents were pipetted directly into the inlet reservoir and withdrawn into the device. This made it possible to use small numbers of cells within small volumes (10^5–10^6 cells mL^{-1}, 1–5 μL aliquots) eliminating cell loss due to dead spaces (syringe and tubing volumes) and cell settlement in stationary syringes.

Cell loading and pairing was achieved using a four-step loading protocol (Fig. 2a). Initially, the first cell population was passively trapped in the single-cell traps by pipetting 1–5 μL of cell solution on the inlet reservoir and drawing into the device. Once the device was saturated, additional cells traveled through the trap array and the inlet reservoir was washed with cell media. The flow was then briefly increased to transfer cells into the larger trap by switching to the high flow syringe pump. Once the transfer was over, the flow was immediately reduced back. Similarly, the second cell population was passively captured and then transferred into the larger traps immediately in front of the previously trapped cells.

Cell preparation and culture

DsRed- and eGFP-expressing NIH3T3 mouse fibroblasts (ATCC) were cultured in DMEM media containing 10% bovine calf serum, 4 mM L-glutamine and 100 U mL^{-1} penicillin and 100 μg Ml^{-1} streptomycin. For fusion experiments, cells were used when 70–80% confluent. Turbo RFP-expressing BA/F3 cells were cultured in RPMI 1640 supplemented with 10% fetal bovine serum, 4 mM L-glutamine and 100 U mL^{-1} penicillin and 100 μg Ml^{-1} streptomycin. Prior to cell loading, cells were suspended in cell media at 5×10^5–10^6 cells mL^{-1} and filtered through a 40 μm cell strainer (BD Falcon).

After cell pairing and fusion experiments, the tubing was removed carefully and additional 20–30 μL cell media was pipetted on both inlet and outlet reservoir to avoid media drying up. Devices were then placed in a manually prepared wet chamber inside cell culture petri dishes and transferred into a standard incubator for long term culture.

Fusion procedure

For electrofusion experiments, electrodes are connected to a high voltage power supply (BTX ECM 830, Harvard Apparatus Holliston, MA) in parallel with a 1 kΩ resistor to facilitate charge discharge after the application of the pulses. Each fusion experiment was conducted with optimized electric field magnitude that was determined empirically by preliminary tests on each day. Once pairing was accomplished, hypoosmolar buffer was flowed past cells for 5 min. The cells were pulsed at varying voltages (1–1.5 kV cm^{-1}) with 5 × 50 μs pulse sequence. Cells were kept in the hypoosmolar buffer for additional 10 min, after which cells were infused with and incubated in cell media for an additional 15 min.

For chemical fusion experiments, PEG-1500 was drawn past cells at 0.1–0.5 μL min^{-1} for 3 min, then cells were incubated in cell medium for 20 min.

Viral fusion experiments were performed using GenomONE-CF EX (HVJ envelope) cell fusion kit(Cosmo Bio USA, Carlsbad, CA), and solutions were prepared according to manufacturer's protocol. Cell pairs were first infused with fusion buffer at 0 °C for 5 min, then with fusion buffer at 37 °C for additional 15 min. Cells were then incubated in cell media for ~20 min for fusion to complete. All experiments were conducted at room temperature (23–25 °C).

Image acquisition and analysis

Time-lapse imaging of fusion experiments were performed on an automated inverted microscope (Nikon Eclipse Ti, Nikon, Melville, NY). Exposure times were determined after cell pairing was completed and kept constant during the experiments. Images were acquired at 4× magnification on a cooled CCD camera (CoolSNAP HQ^2, Photometrics, Tucson, AZ) using Nikon Elements Software (Nikon). Images were taken every 30 s and at each time point both phase and fluorescent images were acquired. Cell capture efficiencies were calculated by the ratio of the number of trapped cells over total cells that entered the device. Total cell number was calculated based on cell concentration and sample volume inputted onto the reservoir. Pairing efficiencies were calculated by determining the number of traps occupied by a single cell of one type paired with the second cell over the entire field of view (~500 traps). Fusion efficiencies were determined by analyzing the fluorescence exchange between correctly paired cells.

Acknowledgements

This research was supported by the Singapore-MIT Alliance.

Notes and references

1 P. Primakoff, H. Hyatt and J. Tredick-Kline, *J. Cell Biol.*, 1987, **104**, 141–149.
2 P. Primakoff and D. G. Myles, *Science*, 2002, **296**, 2183–2185.
3 B. Podbilewicz and J. G. White, *Dev. Biol. Stand.*, 1994, **161**, 408–424.
4 T. Yagami-Hiromasa, T. Sato, T. Kurisaki, K. Kamijo, Y.-I. Nabeshima and A. Fujisawa-Sehara, *Nature*, 1995, **377**, 652–656.
5 E. H. Chen and E. N. Olson, *Trends Cell Biol.*, 2004, **14**, 452–460.
6 C. Saginario, H. Y. Qian and A. Vignery, *Proc. Natl. Acad. Sci. U. S. A.*, 1995, **92**, 12210–12214.
7 J. M. Anderson, *Curr. Opin. Hematol.*, 2000, **7**, 40–47.
8 A. Vignery, *J. Exp. Med.*, 2005, **202**, 337–340.
9 D. Duelli and Y. Lazebnik, *Cancer Cell*, 2003, **3**, 445–448.

10 D. Duelli and Y. Lazebnik, *Nat. Rev. Cancer*, 2007, **7**, 968–976.
11 X. Lu and Y. Kang, *Cancer Res.*, 2009, **69**, 8536–8539.
12 M. Álvarez-Dolado and M. Martínez-Losa, in *Cell Fusion in Health and Disease*, ed. T. Dittmar and K. Zänker, Springer, Netherlands, 2011, vol. 713, ch. 10, pp. 161–175.
13 G. Kohler and C. Milstein, *Nature*, 1975, **256**, 495–497.
14 J. Rosenblatt, D. Kufe and D. Avigan, *Expert Opin. Biol. Ther.*, 2005, **5**, 703–715.
15 C. A. Cowan, J. Atienza, D. A. Melton and K. Eggan, *Science*, 2005, **309**, 1369–1373.
16 S. K. Dessain, S. P. Adekar, J. B. Stevens, K. A. Carpenter, M. L. Skorski, B. L. Barnoski, R. A. Goldsby and R. A. Weinberg, *J. Immunol. Methods*, 2004, **291**, 109–122.
17 T. C. Bakker Schut, Y. M. Kraan, W. Barlag, L. de Leij, B. G. de Grooth and J. Greve, *Biophys. J.*, 1993, **65**, 568–572.
18 J. Wang and C. Lu, *Appl. Phys. Lett.*, 2006, **89**, 234102.
19 A. M. Skelley, O. Kirak, H. Suh, R. Jaenisch and J. Voldman, *Nat. Methods*, 2009, **6**, 147–152.
20 E. W. M. Kemna, F. Wolbers, I. Vermes and A. van den Berg, *Electrophoresis*, 2011, **32**, 3138–3146.
21 M. Gel, Y. Kimura, O. Kurosawa, H. Oana, H. Kotera and M. Washizu, *Biomicrofluidics*, 2010, **4**, 022808.
22 Y. Kimura, M. Gel, B. Techaumnat, H. Oana, H. Kotera and M. Washizu, *Electrophoresis*, 2011, **32**, 2496–2501.
23 N. Hu, J. Yang, S. Qian, S. W. Joo and X. Zheng, *Biomicrofluidics*, 2011, **5**, 034121.
24 L. H. Li and S. W. Hui, *Biophys. J.*, 1994, **67**, 2361–2366.
25 K. Chung, Y. Kim, J. S. Kanodia, E. Gong, S. Y. Shvartsman and H. Lu, *Nat. Methods*, 2011, **8**, 171–176.
26 S. Hong, Q. Pan and L. P. Lee, *Integr. Biol.*, 2012, **4**, 374–380.
27 E. J. Felton, C. R. Copeland, C. S. Chen and D. H. Reich, *Lab Chip*, 2012, **12**, 3117–3126.
28 S. Suri, A. Singh, A. H. Nguyen, A. M. Bratt-Leal, T. C. McDevitt and H. Lu, *Lab Chip*, 2013, **13**, 4617–4624.
29 M. J. Jaroszeski, R. Gilbert, P. G. Fallon and R. Heller, *Biophys. J.*, 1994, **67**, 1574–1581.
30 C. Zhu, G. Bao and N. Wang, *Annu. Rev. Biomed. Eng.*, 2000, **2**, 189–226.
31 U. Marko, T. Katja, H. Rosana, K. Maša and M. Damijan, *Radiol. Oncol.*, 2009, **43**, 108–119.
32 J. Teissie, V. Knutson, T. Tsong and M. Lane, *Science*, 1982, **216**, 537–538.
33 J. Soza-Ried and A. G. Fisher, *Curr. Opin. Genet. Dev.*, 2012, **22**, 459–465.

